Journal of Non-Newtonian Fluid Mechanics 175–176 (2012) 1–9

Contents lists available at SciVerse ScienceDirect

Journal of Non-Newtonian Fluid Mechanics

journal homepage: http://www.elsevier.com/locate/jnnfm

Study of the properties of bubbly flows in Boger-type fluids

J. Rodrigo Vélez-Cordero *, Diego Sámano, Roberto Zenit

Instituto de Investigaciones en Materiales, Universidad Nacional Autónoma de México, Apdo. Postal 70-360, México DF 04510, Mexico

ARTICLE INFO

Article history:
Received 19 December 2011
Received in revised form 6 February 2012
Accepted 13 March 2012
Available online 24 March 2012

Keywords:
Bubble columns
Polymeric solutions
Boger fluids
Bubble clusters
Velocity jump discontinuity

ABSTRACT

Experiments were conducted to study the properties of bubbly flows in elastic fluids with nearly constant viscosity (Boger-type fluids). The effect of gas volume fraction was investigated by injecting bubbles with a narrow size distribution in a vertical column filled with the test fluid. It was found that the dispersion of bubble changes dramatically depending on the bubble size: if the diameter of the bubbles is small, large vertical clusters are formed; on the other hand, the bubble assembly rises in a dispersed manner if the bubble size is increased. To understand the condition for which agglomeration occurs two additional experiments were conducted: the interaction of two side-by-side bubble chains was analyzed; and, the unsteady behavior of the first normal stress difference was studied in a rheometric flow. These analysis suggest that there is a process of accumulation of elastic stress. When the accumulated elastic stress surpasses the viscous repulsive stress, aggregation can occur. Interestingly, the critical diameter at which the bubble dispersion was observed to occur is close to that for which the velocity of an isolated bubble becomes discontinuous: the so-called bubble velocity discontinuity. This suggests that both phenomena share the same fundamental nature. We attributed the change of behavior to the modification of the gas–liquid interface.

1. Introduction

The elasticity is a property that dramatically changes the character of a flow; it challenges the common sense of inertial and viscous effects observed in Newtonian fluids. The stretching that polymer molecules experience when they are subjected to flow can produce, in a macroscopic scale, a negative wake behind cylindrical or spherical bodies [1–4], abrupt changes in the volume–velocity relation of free rising bubbles [5] and aggregation of settling spheres [6,7], to mention a few. In particular, the discontinuity observed in the volume–velocity relation for single bubbles, not seen in inelastic fluids, and the formation of a negative wake in the rear part of the bubble, constitute two topics that have led to many experimental and computational studies aimed to explain the appearance and relation of these two phenomena [3,4,8–14]. There have been two main explanations of the origin of the velocity jump. The first one, which we can call the surface-active agents mechanism, claims that the jump is triggered by a sudden liberation of polymer molecules (or other molecules with surface activity) from the bubble surface. Therefore, this mechanism proposes a sudden change on the bubbles surface: from a rigid to a free surface or slip condition [5,8,15–17]. The fact that solid particles do not present a velocity jump [9], although they can present a negative wake, supports this hypothesis. Depending on the concentration of contaminants or surfactants in the liquid bulk, the change of the boundary conditions can happen either by a sudden change of the intrinsic surface rheology (or, as conceived by Zana and Leal [15], by a rupture of an elastic membrane made by the polymer molecules); or by removal of the surface tension gradient (Marangoni stresses) imposed by a concentration gradient of the adsorbate throughout the bubble surface [16,18,19]. The second explanation, the hydrodynamic mechanism, proposes that the jump is produced by the formation of a negative wake [3,13,14] which causes an action–reaction effect on the bubble velocity. This explanation took importance since the velocity jump was observed to occur at the same bubble volume at which the negative wake appear in shear-thinning viscoelastic fluids [3]. The shear-thinning properties of the fluid additionally contribute to the magnitude of the velocity jump, $H = U_{after}/U_{before}$, where U is the velocity of the bubble either before or after the velocity jump [5]. The velocity discontinuity and negative wake seen in viscoelastic fluids have also been related with the formation of a sharp cusped end on the bubble surface since the three phenomena appear at the same critical bubble volume V_{crit} [3,4,10]. In another context, lateral motion of moving bodies due to normal elastic stresses have also shown to bear some relation with the boundary conditions at the interface. Joseph et al. [6], for example, reported that two abreast particles can experience attraction when moving in viscoelastic fluids if the initial separation between them is below a critical one. On the other hand, Sullivan et al. [20] observed that transverse instabilities can occur in bubbles traveling in viscoelastic channel flows

* Corresponding author. Tel.: +52 55 5611 9123; fax: +52 55 5622 4602.
E-mail address: jvelez@iim.unam.mx (J. Rodrigo Vélez-Cordero).

0377-0257/$ - see front matter © 2012 Elsevier B.V. All rights reserved.
http://dx.doi.org/10.1016/j.jnnfm.2012.03.008

as long as the gas–liquid interface is immobilized by the addition of surfactants, otherwise, the slip condition will reduce the normal stresses generated in the liquid by shear deformation.

Motivated by the fact that most of the studies in non-Newtonian bubbly flows have been conducted using shear-thinning viscoelastic fluids [21,22], the objective of the present work is to study the relation between the single bubble kinematics with the collective behavior of many bubbles rising in Boger-type fluids, i.e., discarding the shear-thinning effects. We recently found that, for the case of shear-thinning inelastic fluids, the bubbly flow develops strong clustering in a passive way depending on the Reynolds and Eötvös numbers of individual bubbles [21,22]. The present paper is organized as follows: in Section 2 some relevant dimensionless numbers are revised concerning the single bubble motion, the experimental setup is presented in Section 3, the results section is divided in two parts: Section 4.1 for single bubbles and Section 4.2 for the bubble-swarm experiments. In Section 5 we discuss the origin of the velocity jump discontinuity seen in the single bubble experiments and the effect that this phenomenon may have on the dispersion of bubbly flows. The effects of the accumulation of normal forces due to the consecutive passage of bubbles in the dispersive character of bubbly flows is also discussed here by studying the interaction of two parallel bubble chains and the unsteady behavior of the first normal stress difference. The conclusions are presented in Section 6.

2. Dimensionless numbers

Before we describe the experimental study, we would like to briefly discuss the relevant numbers for this investigation. One important aspect in the study of single bubbles rising in viscoelastic fluids has been the estimation of the critical bubble size at which the velocity jump occurs [5]. Since the balance between the elastic, viscous and surface forces plays a significant role in the bubble final shape and surface conditions, most of the researchers have used a combination of these forces to define an appropriate dimensionless number [4,5,12,17,23].

The relevance of the elastic stresses are frequently compared with the shear stresses using a measure of recoverable shear:

$$\Pi = \frac{N_1}{2\tau} \tag{1}$$

where N_1 is the first normal stress difference and τ the shear stress. The 1/2 factor is introduced for convenience, as we will see below. In the case of infinite extensible elastic fluids with constant viscosity, N_1 can be related with the relaxation time of the fluid using the material function of an Oldroyd-B fluid submitted to steady shear flow [24]:

$$\lambda_1 - \lambda_2 = \frac{\Psi_1}{2\eta_o} \tag{2}$$

where Ψ_1 is the first normal stress coefficient ($\Psi_1 = N_1/\dot{\gamma}^2$, $\dot{\gamma}$ being the shear rate), η_o the zero-shear viscosity of the fluid, λ_1 and λ_2 the relaxation and retardation times of the fluid respectively. Knowing that $\lambda_2 = \lambda_1\eta_s/\eta_o$ and $\eta_o = \eta_s + \eta_p$ for an Oldroyd-B fluid, η_s and η_p being the solvent and polymer contribution to the total viscosity, and considering only the polymer contribution for the steady shear stress in the stress ratio ($\eta_p\dot{\gamma}$); Eqs. (1) and (2) can be related in order to convert the stress ratio to a characteristic time ratio or Weissenberg number:

$$Wi = \lambda_1\dot{\gamma} \tag{3}$$

where λ_1 is equal to

$$\lambda_1 = \frac{\Psi_1}{2\eta_p} \tag{4}$$

For the case of bubbles rising at small but finite Reynolds numbers, an "effective" shear rate can be computed considering the ratio U/r_b, U and r_b being the terminal velocity and bubble radius respectively.

The ratio of the viscous and interfacial forces can be estimated using the capillary number defined as:

$$Ca = \frac{\eta_o U}{\sigma} \tag{5}$$

where σ is the surface tension. Note, however, that a unique value of the surface tension cannot describe the nature of the velocity jump according to the surface-active agents mechanism, in particular when Marangoni stresses are present. Rodrigue et al. [25] showed that the stress generated at the interface due to the nonuniform distribution of the surface tension value can be approximated considering a surface tension difference $\Delta\sigma = \sigma_s - \sigma$, where σ_s and σ are the surface tension value of the solvent and solution respectively. The viscous and interfacial stresses can be now related using a surface tension gradient by means of the Marangoni number:

$$Ma = \frac{\Delta\sigma}{\eta_o U} = \frac{\Delta\sigma}{r_b\tau} \tag{6}$$

where the characteristic shear rate $\dot{\gamma} = U/r_b$ has also been considered.

In order to couple the interfacial stresses with the elastic ones, Soto et al. [4] proposed to group the dimensionless recoverable shear with the Capillary number giving the following dimensionless number:

$$\Pi_1 = \frac{4N_1}{2\tau}Ca = \frac{2N_1 r_b}{\sigma} \tag{7}$$

On the other hand, Rodrigue et al. [17] proposed a dimensionless number considering the Capillary, Weissenberg and Marangoni numbers in the form:

$$\alpha = \frac{CaWi}{Ma} \tag{8}$$

that is, adding the surface tension difference. Later on, Rodrigue and De Kee [23] proposed a scaling parameter β to relate the elastic and surface tension difference with the critical radius via the Bond number, where the Bond number and the parameter β are defined as:

$$Bo = \frac{\rho g r_b^2}{\sigma} \tag{9}$$

$$\beta = \left(\frac{\sigma}{\Delta\sigma}\right)^{0.1}\left(\frac{\tau r_b}{\sigma}\right)^3\left(\frac{\sigma}{N_1 r_b}\right) \tag{10}$$

where ρ and g are the liquid density and the gravity, respectively.

All the dimensionless numbers and relations mentioned so far assume that the elastic stresses act on the bubble surface through shear flow. It is well known, however, that close to the south pole of the bubble the flow is extensional, so we expect to have a combination of normal forces coming from both flows in the rear part of the bubble. In this context, Pilz and Brenn [12] used the physical properties of the fluids grouped in the Morton number and a new dimensionless number Π_2 that considers the extensional relaxation time in order to estimate the critical diameter (in terms of a critical Eötvös number, Eo = 4Bo). The Morton and Π_2 numbers are defined as:

$$Mo = \frac{g\eta_o^4}{\rho\sigma^3} \tag{11}$$

$$\Pi_2 = \frac{g^{1/3}\lambda_E\rho^{1/4}}{\sigma^{1/4}} \tag{12}$$

where λ_E is the extensional relaxation time of the fluid. These dimensionless numbers were related by means of an empirical

equation using a non-linear least square method; hence, we expect that the analysis of Pilz and Brenn will primary serve to compare fluids with a similar set of physical values.

3. Experimental setup

3.1. Column and bubble generation

The bubble-swarm and bubble-chain experiments were conducted in a rectangular column made of transparent acrylic with an inner cross section of $5 \times 10\,cm^2$. The column was filled with the test liquid up to a level of 100 or 140 cm measured from the base plate. The 140 cm level was used for the case of the bubble-swarm experiments. Three capillary banks were used to produce different bubbly flows each having a different mean bubble size (2.1, 3.1 and 4.2 mm). Pure nitrogen was introduced to the column through the capillary bank via a gas chamber. For the generation of two parallel bubble chains, the capillary bank and the gas chamber were replaced by a setup consisting in one capillary inserted through the bottom of the column, using a sealed feedthrough (*Spectite Series PF*), at the center of the base plate, and a second capillary inserted through the side wall, using an elbow and another feedthrough connector. In this manner the initial horizontal separation between bubbles could be varied. The injection rate of the bubbles (now filled with air) was controlled using a syringe pump (*KDScientific 100L*). The details of the capillary banks design can be seen in [21,22]. Since the gas–liquid mixture showed a prevalent non-coalescing behavior, the standard deviation of the bubble diameter was small (around 10% of the mean value), hence a nearly monodispersed condition was achieved.

The study of single bubbles was conducted in a cylindrical tube having a diameter D of 9 cm; a detailed description of the device can be found in [4]. The ratio d_b/D, d_b being the bubble diameter, was in most of the cases less than 0.07. The bubbles were released 1–5 min after each measurement allowing the fluid to relax and achieve the stagnant condition. The single bubble generator used in this work form bubbles with an arbitrary volume, i.e., the bubble volume varies arbitrary in each consecutive experiment. The repeatability of the measurements was corroborated by the fact that the volume–velocity curve showed a monotonic tendency in all the volume range (see Section 4.1).

3.2. Working fluid

In this work we used a Boger-type fluid in order to minimize the shear-thinning effects. Such fluid was made by dissolving 400 ppm (0.04 wt.%) of ionic polyacrylamide (Paam, *Aldrich 181277*, $M_w = 5 \times 10^6$ g/mol) in a 80/20 (v/v) glycerin–water mixture. We added to the solution 9.8 g/l of $MgSO_4$ (*2500-01 J.T. Baker*) to reduce bubble coalescence [26]. According to these authors, when salts form solvation structures with the solvent they reduce the drainage of the liquid film that appears when two bubbles become close to each other. The viscosity of this solution was high enough to develop non-linear viscoelasticity but low enough to allow the generation of individual bubbles (bubbly flow). The dependence of the viscosity η and the first normal stress difference N_1 with the shear rate was measured with a *TA Instruments AR1000N* rheometer having a cone-plate geometry (60 mm, 2°, 65 μm of cone truncation). The flow curves are shown in Fig. 1. The figure also shows the viscosity of a Newtonian reference solution formulated to have the same viscosity as the Boger fluid. The polymer concentration parameter c for this fluid, defined as the ratio of the polymer and solvent contribution to the zero-shear viscosity, $c = \eta_p/\eta_s$, is 1.27. The flow index value, calculated by fitting the viscosity data with the power-law model, is 0.96. A summary of the physical properties of the Boger fluid is shown in Table 1. The surface tension was measured with a DuNouy ring (diameter of 19.4mm, *KSV Sigma 70*). The relaxation time λ_1 shown in the table correspond to the inverse of the frequency value at which the dynamic moduli curves G' and G'' intersect. The oscillatory moduli were obtained experimentally by a Fourier transform of the stress relaxation curves measured with an AR-G2 rheometer of controlled stress [21,27]. Although we did not conduct measurements of the extensional properties for this fluid, the extensional relaxation time can be estimated using the work of Stelter et al. [28]. They reported the relaxation times and steady extensional viscosities for several polymeric solutions using an elongational device. In that work, the relaxation time was measured from the diameter decrease of an elongated thread [29] formed between two moving plates, i.e., the extensional rate in the liquid is given by its own physical properties provided that the separation rate between the plates is larger. We set a value of 0.55 s as the relaxation time, λ_{ext}, for our Boger-type fluid according to the data given by these authors for a similar fluid (400 ppm of nonionic polyacrylamide, $M_w \approx 9 \times 10^6$ g/mol, dissolved in a 80/20 (w/w) glycerin–water mixture).

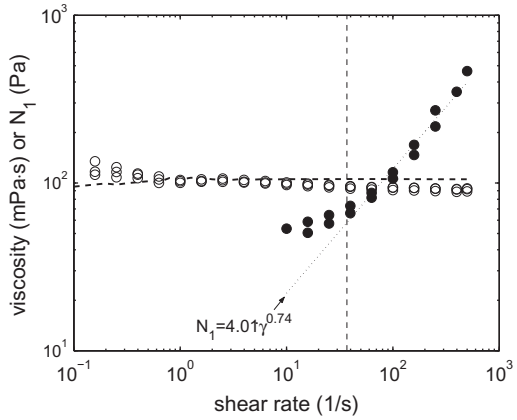

Fig. 1. Flow curve of the Boger fluid and the Newtonian reference solution. (–) Viscosity of the Newtonian fluid: 83% glycerin–water mixture having 9.8 g/l of $MgSO_4$; (○) viscosity and (•) first normal stress difference of the Boger fluid. Vertical line: shear rate at which the velocity jump occurs for single bubbles. The dotted line denotes a power law fitting made to the first normal stress difference in the range of $30 < \dot{\gamma}[s^{-1}] < 500$.

3.3. Bubble size and velocity measurement

Bubbles rising in elastic fluids can show a teardrop shape. Therefore, the second centroid theorem of Pappus was used to compute the volume V:

$$V = 2A\pi r_{centroid} \tag{13}$$

where A is the half of the projected area of the bubble, considering its axis of symmetry, and $r_{centroid}$ is the length between the axis of symmetry and the centroid of A. The equivalent diameter d_b of the bubbles was estimated using Eq. (13) and the sphere volume $\pi d_b^3/6$. The image analysis was made in *Matlab*©.

The measurement of the bubble vertical velocity was made with a high speed camera (*MotionScope PCI 8000s*), using a stationary frame in the case of single bubbles and bubble swarms, and a moving frame for the case of bubble chains. For the first case, the terminal velocity was estimated dividing the total displacement of the bubble in the visualization window (480 × 420 pixels, the projected area of the bubble representing 2% of the total area) by the elapsed time between the corresponding images. The image resolution was 11 pixels/mm. For the case of bubbles chains, bubble

Table 1
Physical properties of the Boger fluid. $\eta_{o,a}$ stands for the viscosity of the polyacrylamide dissolved in an aqueous solvent (water) at the same polymer mass fraction of the glycerin–water solution. This value was used to compute the critical diameter in Eq. (14). The extensional relaxation time λ_E was estimated using the results reported by [28]. The viscosity and surface tension measurements were done at a controlled temperature of 23 °C.

ρ (kg/m^3)	η_o (Pa s)	σ (mN/m)	$\Delta\sigma$ (mN/m)	η_p/η_s	$\eta_{o,a}$ (Pa s)	λ_1 (s)	λ_E (s)
1206.7	0.117	55.6	7.38	1.27	0.0047	0.53	0.55

vertical trajectories were followed by the high speed camera mounted on a vertical rail activated by a DC motor [22]. We took the images at a speed of 500 frames/s in the stationary frame and 60/s in the moving frame.

The liquid velocity fields produced by the bubbly flow were obtained with a standard 2D particle image velocimetry (PIV) technique; the resulted vector field was composed by 62×62 sub-areas, each having a velocity vector.

4. Results

4.1. Single bubbles

The terminal velocity of single bubbles U, as a function of the volume V, for the Boger fluid and the Newtonian reference solution is shown in Fig. 2. The presence of a velocity jump discontinuity is evident ($H = 1.3$, $V_{crit} = 19.3$ mm^3) and is accompanied by the formation of a small cusp at the rear part of the bubble (Fig. 3). The critical diameter at which the velocity jump occurs together with other parameters of interest calculated at $\dot{\gamma}_{crit}$ are shown in Table 2. In this case the Wi_{crit} and λ_{crit} were calculated using Eqs. (3) and (4).

The flow field in the liquid left by a single bubble having a volume above the critical one is shown in Fig. 4. The velocity field is characterized by an absence of a negative wake, showing that the velocity jump is not a result of a change in the flow configuration. This feature was corroborated for the whole bubble size range tested in this work ($0.35 < V < 180$ mm^3).

4.2. Bubble swarms

Fig. 5 shows photographs of the typical flows produced by the three capillary banks at approximately the same Φ_g for the Boger and Newtonian solutions. Note that the bubble swarms shown in

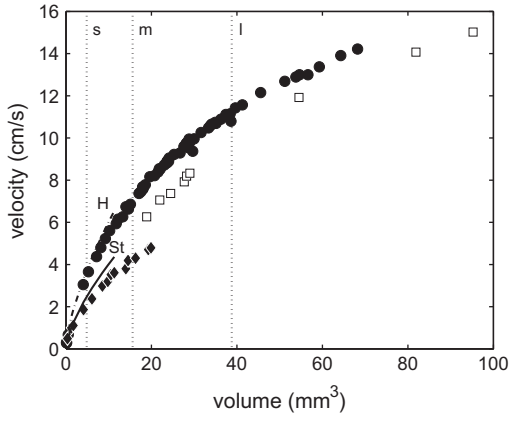

Fig. 2. Single bubble velocity as a function of the bubble volume; (•) Newtonian fluid; values before (♦) and after (□) the velocity jump in the Boger fluid. The average Reynolds ($\rho U d_b/\eta$) and Weber ($\rho U^2 d_b/\sigma$) number at the critical volume is 2.2 and 0.2 respectively. The dotted-dashed and continuous lines denoted by H and St, respectively, refers to the Hadamard and Stokes velocities. The horizontal lines shows the mean bubble volume obtained in the bubbly flows (Section 4.2) for the small (s, 4.8 mm^3), medium (m, 15.6 mm^3) and large (l, 38.8 mm^3) bubbles.

Fig. 3. Typical bubble shape before (left image) and after (right image) the velocity jump.

Table 2
Properties of the Boger fluid at the critical volume. All the data were calculated using the average of the values before and after the jump. λ_{crit} was calculated using Eq. (4).

d_{bcrit} (mm)	$\dot{\gamma}_{crit}$ (s^{-1})	λ_{crit} (s)	Wi_{crit}	Ca	Bo	α	Bo/β
3.3	31.5	0.65	20.17	0.11	0.59	1.55	871

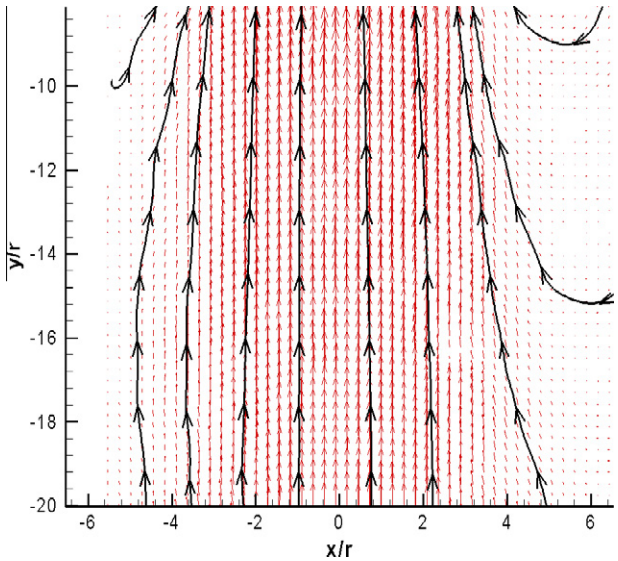

Fig. 4. Velocity field obtained by PIV of the wake left by the passage of a single bubble (having a volume above the critical one) in the Boger fluid. $V = 71$ mm^3. The Reynolds and Weber number are 8 and 1.8 respectively. The lines show some of the flow streamlines. The center of the bubble is located at (0,0). The grid coordinates were normalized with the bubble radius.

Fig. 5a–c have a volume below the critical one, according to Fig. 2, while the bubbles shown in Fig. 5d–e correspond to the $V > V_{crit}$ case. Unlike the Newtonian case, the bubbles with $V < V_{crit}$ form vertical clusters in the Boger fluid which in time evolve into a single large vertical cluster, hence, leaving the rest of the column for the liquid circulation. The gas segregation cause a rapid fall of the gas fraction and an increase of the mean bubble swarm velocity U_{SW} with respect to that of a single one, U_{SI} ($U_{SW}/U_{SI} \approx 9$). For the case when $V > V_{crit}$, the bubbles disperse, as shown in Fig. 5d. In this case the gas fraction was increased up to a value of 0.75% producing only a slight increase in the velocity ratio ($U_{SW}/U_{SI} \approx 1.3$). Fig. 5e shows a zoom of the large bubbles ($V > V_{crit}$). We can see that a small cusp is formed in the south pole of the bubbles. As

(a) Newtonian fluid, small bubbles $V = 4.8mm^3$, Φ_g=0.66%

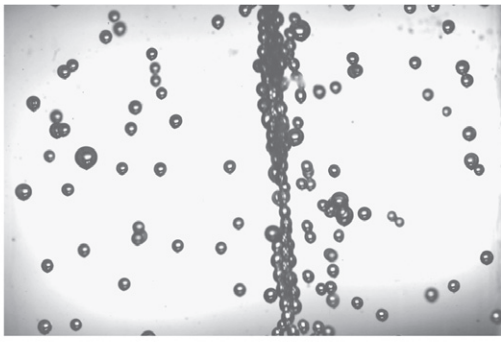

(b) Boger fluid, small bubbles $V < V_{crit}$, $\Phi \approx 0.5\%$, $V = 4.8mm^3$

(c) Boger fluid, medium bubbles $V < V_{crit}$, $\Phi \approx 0.5\%$, $V = 15.6mm^3$

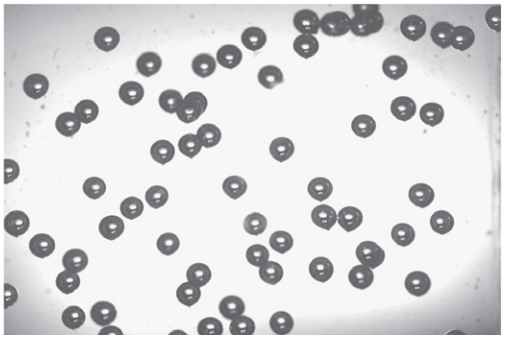

(d) Boger fluid, large bubbles $V > V_{crit}$, $\Phi = 0.6\%$, $V = 38.8mm^3$

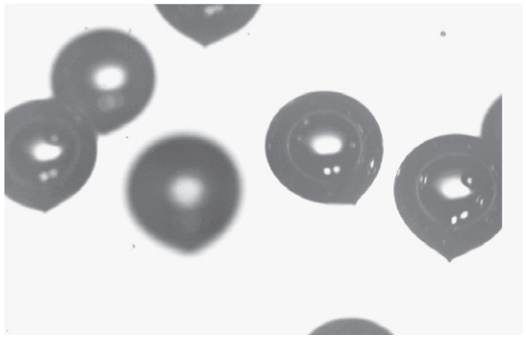

(e) zoom of (d)

Fig. 5. Bubbly flow pictures of the Newtonian and Boger fluids taken at a similar gas volume fraction. The size of the pictures are about 5 × 3 cm for (a), 8 × 5 cm for (b) and (d), 2.6 × 2.3 for (c) and 1.7 × 1.1 cm for (e). The gas volume fractions for the (b) and (c) cases correspond to the values measured at the beginning of the bubbly flow.

mentioned previously, such cusped end shape has been related with a possible change of the interface mobility and cleansing of the bubble interface at the critical volume [4,5].

5. Discussion

5.1. Effects of the velocity jump discontinuity

In the following, we will discuss the causes of the velocity jump seen in the single bubble experiments and then the effects that it can have on the dispersive character of the bubbly flow.

The explanation of the origin of the velocity jump in this fluid must be closer to the surface-active agents hypothesis. First of all, the velocity discontinuity is not a 'jump' in the sense of increase but in the sense of a velocity recovery. In Fig. 2 it can be seen that after the jump, the velocity values become closer to the Newtonian ones, suggesting that a partial release of the extra stress component (elastic) is occurring on the bubble surface. Interestingly, the ratio of velocities after and before the jump is 1.3, i.e., close to the theoretical Hadamard–Stokes ratio (1.5). Secondly, this fluid has a surface tension difference of $\Delta\sigma = \sigma_s - \sigma = 62.98 - 55.6 = 7.38$ mN/m, revealing that the polyacrylamide used has surface activity. The critical diameter, d_{bcrit}, could not be predicted according to the Capillary (Ca = 1) and Bond (Bo = 1) criteria (see Table 2 and Rodrigue's paper [5]). The dimensionless Π_1 number, proposed by [4], was also unable to predict the correct value. The dimensionless number α and the scaling parameter β, which take into account the surface tension difference, predicted a critical diameter close to the experimental one. At $\alpha = 1$, i.e., the hypothetical value at which the velocity jump occurs [17], the corresponding diameter deviates 8% from the experimental value (in contrast, for example, the predicted

value deviates 31% at Bo = 1). In the case of the parameter β, Rodrigue and De Kee [23] noted that the velocity jump occurs when $Bo/\beta \approx 1300$. In our case the jump occurred at $Bo/\beta \approx 1000$.

We also computed the critical diameter using the dimensionless number Π_2 proposed by [12] and their empirical equation:

$$\mathrm{Eo}_{crit} = 5.4801 \frac{\Pi_2 - 9.9381^{0.9087}}{\mathrm{Mo}^{0.3268}} \left(\frac{\eta_{o,a}}{\eta_o}\right)^{1.2144} \left(\frac{[\eta_o]}{[\eta_a]}\right)^{1.4389} \quad (14)$$

where Eo_{crit} is calculated using the critical diameter, $\eta_{o,a}$ and η_o are the zero shear viscosities of the aqueous and non-aqueous solutions at the same polymer mass fraction (see Table 1), $[\eta_o]$ and $[\eta_a]$ are the intrinsic viscosities of the non-aqueous and aqueous solutions respectively. The intrinsic viscosity is defined as $[\eta] = \lim_{\varphi\to 0}(\eta - \eta_s)/\eta_s\varphi$, where η is the viscosity of the solution, η_s the viscosity of the solvent and φ the volume fraction of the solute in the solution (the density of the polyacrylamide powder is 0.75 g/ml according to product specifications). Since we have all the physical data, the critical diameter (using Eq. (14)) was calculated: 2.82 mm against the real value of 3.3 mm, representing a deviation of 15%. Such agreement encourage the use of Eq. (14), which consider the extensional properties of the fluids. We need to point out that the present form of Eq. (14) do not permit a clear understanding of the interplay between the extensional properties of the fluids and the boundary conditions at the interface. It is also not surprising that our results are similar to the ones given by [12] since both works employed similar fluids.

Besides comparing the critical size obtained in this work with the available criteria found in the literature, we also need to include a note regarding the computation of the critical size itself according to these criteria. The issue of computing dimensionless numbers that include normal stress differences, such as Π_1 or β, is that the onset of the non-linear viscoelastic response often occurs at the same shear rate at which the velocity jump occurs (see Fig. 1 and [3,4]), implying that N_1 may not be measurable yet at these shear rates. In view of these experimental limitations, some authors have considered different ways to extend the N_1 curve to low shear rates. For example, Soto et al. [4] used a constitutive equation (Bautista–Manero–Puig Model), while Rodrigue and De Kee [23] employed oscillatory moduli to calculate steady state data. We can expect then that agreement with the critical size criterium proposed by each of these authors will be also linked to the specific model employed. In this work, the first normal stress difference N_1 at the critical shear rate was directly taken from the flow curve (Fig. 1).

Once we have highlighted the importance of the gas–liquid interface changes in the kinematics of single bubbles, we now analyze if such changes can actually modify the dispersive character of bubbly flows rising in Boger fluids.

We saw in the results that vertical bubble clusters can be formed if the liquid experience consecutive deformations due to the passage of bubbles. What is intriguing here is that the gas dispersion happens in a narrow range of bubble sizes (3.1–4.2 mm). Liu and Joseph [30] have shown that the transition from viscoelastic to inertia dominated flows can occur in a narrow range of Reynolds numbers due to the pressure redistribution around rigid objects (the elastic forces are compressive in nature [31]). That is why elongated bodies can turn their relative orientation (from vertical to broadside-on) when the Reynolds number is typically higher than one (supercritical speeds). In our case, there are some experimental facts suggesting that this mechanism does not applies to the clustering-dispersion transition shown here. First, in order to observe lateral attraction between two rigid spheres when viscoelasticity dominates the flow, as in [6], or vertical alignment of elongated bodies, as in [30], the relaxation time of the Maxwell unit must be greater than the retardation time of the parallel dashpot, that is, $\lambda_2 \ll \lambda_1$, or equivalently, $\eta_s/\eta_o \ll 1$. This is not the case for the Boger-type fluid used here in which $\lambda_2 = \mathcal{O}(\lambda_1)$. The weak elastic response of our Boger type fluid was corroborated by additional experiments (not shown here) designed to follow the trajectory of just two bubbles rising side-by-side having a close initial distance ($\delta/d_b \sim 3.7$, δ being the separation distance between bubble centers). In that particular case, we did not observed attraction between bubbles having the size range studied here. The difficulty in relating the formation of long vertical chains at supercritical speeds or the bubble dispersion with the increase of inertia can also be shown by considering the different Reynolds numbers of the flows. For example, the Reynolds number reached by the clustered case seen in Fig. 5c is around 7, while the unclustered case formed by the large bubbles (Fig. 5d) is 5.3, that is, the opposite of what we would expect if inertia overpasses viscoelastic stresses.

Besides the Reynolds criterium, Liu and Joseph noticed that the orientation change of elongated bodies also occurs when the Mach number $M = (U/C)$ is around one, C being the shear wave speed and equal to $\sqrt{\frac{\eta}{\rho\lambda_1}}$. In our case, we do not dispose shear wave speed data of the Boger-type fluid used here measured with the technique prescribed by [30]. If we use instead the relaxation time given by Eq. (4) to compute C, we will obtain a Mach number of 3.5 and 5.1 for the clustered (small bubbles) and disperse (large bubbles) flows respectively, and a shear wave speed of around 3 cm/s (the value of C of the polyacrylamide solution used by [30] was 16.7 cm/s). Once again, the Mach criterium is not sufficient to explain the clustering-disperse transition described here.

The other explanation that we can address for the bubble dispersion is the change of the gas–liquid interface. Indeed, we can see that the corresponding bubble sizes for the clustered and disperse cases (2.1 and 3.1 for the former and 4.2 for the latter, see Fig. 2 for reference) are below and above the critical diameter (3.3mm) for which single bubbles experience the velocity jump discontinuity. In Section 4.1 we showed that the velocity curve of the Boger fluid, compared with the Newtonian one, indicates a partial release of the extra elastic force from the bubble interface. In this context, we can argue that the dispersion observed in the bubbly flow is a result of the decrease of the normal forces exerted on the bubbles due to a change of the boundary properties, therefore, decreasing lateral migration and bubble clustering. The last question that remains for us to clarify is therefore how does the accumulation of normal stresses due to the consecutive passage of bubbles leads to the formation of bubble pairing, and, subsequently, bubble clustering.

5.2. Effects of the accumulation of elastic stresses

In order to investigate the accumulation of stresses in the fluid due to the semi-continuous deformation applied by the passage of bubbles, we released two parallel bubble chains (individual bubbles with $V < V_{crit}$) in the rectangular bubble column having an initial horizontal separation distance of 1 cm (this was the smallest separation distance we could achieved with the present experimental setup). Fig. 6 shows pictures of two bubble chains released in the Boger-type fluid for two different values of the injection rate ($1/T$): 60 ml/h ($T = 0.17$ s) and 130 ml/h ($T = 0.08$ s), respectively, T being the injection period between consecutive bubbles.

In the first case we can see that there is no visible attraction between bubbles coming from different chains, although there is some interaction between bubbles located in the same chain. Such bubble in-line interactions have also been observed in Newtonian flows [32]. When the injection period is decreased (Fig. 6c and d), some bubble interaction between chains begins to occur. This indicates the appearance of compressive forces which leads the union of two abreast bubbles. Note that for two spherical bodies moving side-by-side at low Reynolds numbers the force is repulsive due

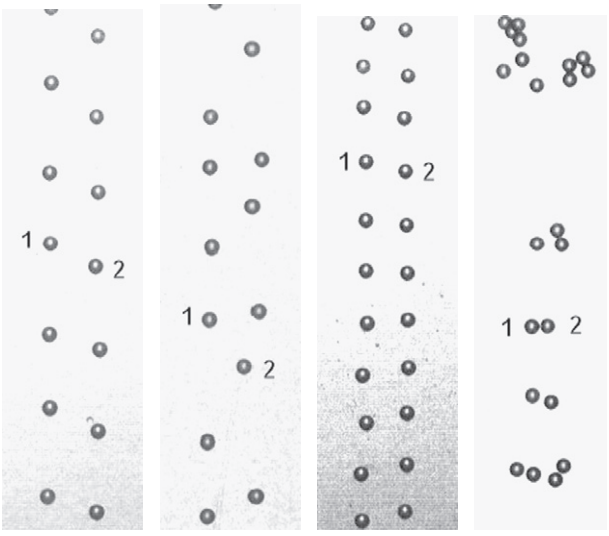

Fig. 6. Bubble chains produced at different gas flow rates with bubbles having a $V < V_{crit}$. Separation between bubbles chains: 1 cm; $d_b = 2.1$ mm, $Re \approx 2.3$. The numbers in the figure denotes the position of two bubbles at different times.

to converging streamlines [33]. We can argue then that there is a gradual accumulation of normal elastic stress due to the consecutive passage of bubbles. Such accumulative process was first suggested by Li and coauthors [34]. These authors performed a series of experiments in order to simulate the consecutive passage of bubbles through a fluid and measure the shear stresses forming on it (a methodology coined as "rheological simulations"). In this work the same methodology was employed to see if the Boger-type fluid was also capable, as the fluids employed by these authors, to show residual stresses. It turned out that the viscosity of the Boger fluid was not sufficiently high to generate residual shear stresses that allow us to distinguish differences between this fluid and its Newtonian counterpart. We decided then to conduct unsteady measurements of the first normal stress difference, N_1. A controlled-deformation rheometer (*ARES-RFS III, TA Instruments USA*) was programmed to apply a steady shear rate to a fluid sample using the cone-plate geometry, starting from rest. The shear rate corresponded to that of a bubble ascending freely ($\dot{\gamma} = U/r = 72.3\ s^{-1}$, U being the vertical bubble velocity for the case presented in Fig. 6c). The evolution of N_1 was determined throughout the process until a steady state was reached. After a certain time, the deformation was stopped to also determine the relaxation of N_1 with time. Fig. 7 shows the N_1 values normalized by the steady state value as a function of time.

The increasing values of N_1 in the initial phase can be fitted to an empirical saturation equation of the form:

$$N_1 = \frac{N_{max}(t - t_o)}{\lambda_{growth} + t - t_o} \tag{15}$$

where N_{max} is the maximum steady N_1 value reached by the initial slope before the overshoot; λ_{growth} is the time for which the $Nmax/2$ value is reached and t_o is the reference time (when N_1 has a zero value). On the other hand, the relaxation curve can be modeled considering an exponential decay equation:

$$N_1 = N_{in}\left[\sum_{i=1}^{2} a_i e^{-(t-t_{in})/\lambda_i}\right] \tag{16}$$

where N_{in} is the initial value at the time t_{in} at which the shear deformation is stopped, λ_i are the relaxation times and a_i are constants. Assuming that the unsteady stress profile is the same whether or

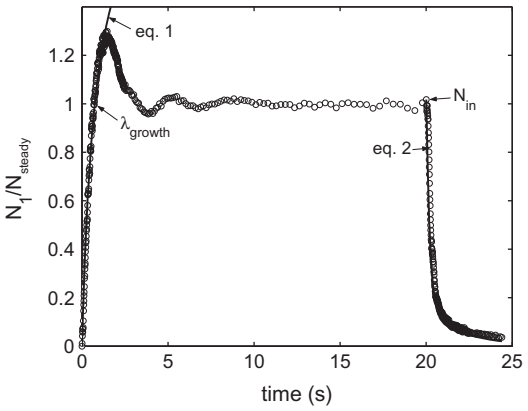

Fig. 7. Normal stress values of the Boger fluid taken at a steady shear rate of 72.3 s^{-1}. The deformation rate was stopped after 20 s. The original curve was filtered in order to eliminate mechanical oscillations of the rheometer motor. The parameters depicted in the figure corresponds to Eqs. (15) and (16): $N_{steady} = 32$ Pa, $N_{max} = 65.9$ Pa, $\lambda_{growth} = 0.79$ s, $a_1 = 0.866$, $\lambda_1 = 0.208$ s, $a_2 = 0.133$, $\lambda_2 = 2.303$ s.

not the steady state has been reached, the accumulation of normal stress due to the consecutive passage of the bubbles can therefore be approximated using these two equations alternately and considering the values of the injection period T and the characteristic bubble time $t_b = 1/\dot{\gamma}$. For instance, Eq. (15) is used until the time t_b is reached, then we continue computing the stress with Eq. (16) making $t_{in} = t_b$ until the time $t_b + T$ is reached. After this, we use Eq. (15) again (updating the t_o value) up to a time $2t_b + T$ and so on. Fig. 8 shows the rheometric values of the normal stress difference in the form N_1/N_{steady} as a function of the normalized time t/t_b together with two curves obtained from Eqs. (15) and (16). The value of the repulsive stress produced by the converging streamlines in between two spherical bodies is also shown in Fig. 8 according to the equation proposed by Vasseur and Cox [33]:

$$S_L = -\frac{9}{2}\eta U(\delta\delta^*)^{-1}\left[2 - (\delta^* + 2)e^{-\frac{1}{2}\delta^*}\right] \tag{17}$$

where δ is the separation distance between bubble centers and $\delta^* = \rho\delta U/\eta$, U being the bubble velocity within the chain. This value represents the stress that the surrounding liquid must have in order to drive the union of two bubbles rising side-by-side.

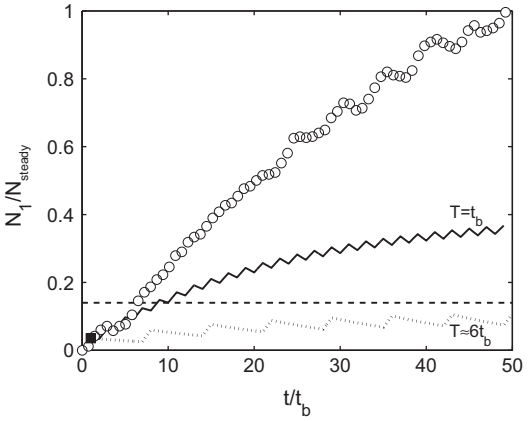

Fig. 8. Normalized normal stress difference, N_1/N_{steady}, as a function of the normalized time t/t_b ($t_b = 0.01382$ s); (○) rheometric values; dotted and continuous lines: estimated values of the normal stress using Eqs. (15) and (16) for $T \approx 6t_b$ and $T = t_b$ respectively; (■) normal stress value produced by the passage of a single bubble. The dashed horizontal line corresponds to the normalized repulsive stress generated by two abreast spherical bubbles according to Eq. (17). The maximum value of the abscissa is less than $\lambda_{growth}/t_b = 57$.

The dotted curve in Fig. 8 represents the experimental case showed in Fig. 6c ($T \approx 6t_b$). For the case of bubbly flows, the T/t_b ratio is above the value found for the bubble chains and close to the $T/t_b = 1$ condition (continuous line in Fig. 8). Note that as the injection period T approach the characteristic time of the bubble, the repulsive stresses between bubbles are easily surpassed by the accumulated normal stresses. This is the reason why we can observe bubble clustering in the bubbly flows and not in the bubble chains experiments when the time ratio T/t_b is high. We understand that the behavior of bubbly flows, compared with the behavior of bubble chains, is governed by a more complex interaction between the disperse and continuous phase. A more accurate estimation of the behavior of bubbly flows starting from the behavior of two bubble chains could be obtained if the former are considered as a collection of many bubble chains. Finally, note that none of the curves shown in Fig. 8 representing different time ratios, including the case when $T/t_{b\to\infty}$ (single bubble case, black square in Fig. 8), reach the rheometric steady value of N_1. This is an important observation since such value is often used in the analysis of unsteady flows.

We want to mention that the effects of elasticity found in this work, i.e., that the elastic stresses promote segregation of the disperse phase, contrast with the results found in elastic fluids having low viscosities values ($\eta \sim 4$ mPa s). For example, Olivieri et al. [35] recently found that elasticity can actually stabilize the homogeneous regime of bubbly flows produced in water–glycerin mixtures having 0.1% of polyethylene oxide. Although these authors related such stabilization to the possible appearance of a negative wake, we think that the explanation of such effect is not clear yet since it is impossible that a liquid having such viscosity values could promote the formation of a flow inversion in the flow field.

6. Conclusions

The size and velocity of bubbles rising in an elastic fluid with nearly constant viscosity was measured. Different experimental setups were used to study the rise of one bubble, two parallel bubble chains and bubble swarms. For the case of single bubbles, a velocity jump discontinuity in the volume–velocity plot was observed without the appearance of a negative wake, showing that the two phenomena are not always related. When compared with the single bubble curve obtained for the Newtonian reference solution, the velocity jump indicates that a partial release of the extra stress is occurring at the bubble interface. Moreover, the magnitude of the velocity jump (1.3) is close to the theoretical ratio of the Hadamard and Stokes velocities (1.5).

The dispersion of bubble swarms rising in this Boger-type fluid turns out to changes dramatically depending on the bubble size: if the diameter of the bubbles is small, large vertical clusters are formed; on the other hand, the bubble assembly rises in a dispersed manner if the bubble size is increased. It was found that the bubble size at which the gas dispersion occurs is close to the critical diameter for which the velocity of an isolated bubble becomes discontinuous, suggesting that bubble dispersion is due to a change of the properties of the bubble interface.

Finally, the study of the interaction of two bubble chains rising side-by-side showed that lateral attraction between bubbles its also dependent on the injection period between bubbles. This suggest that an accumulative process of elastic stresses is taking place which, after certain number of deformations, surpass the repulsive forces generated by the streamlines of neighboring bubbles.

In view of the results obtained in this work, we can say that the formation of small bubbles is not always the most efficient way to increase the mass transfer in viscoelastic flows. Indeed, while in Newtonian liquids high values of the interfacial area per unit volume (α) can be generated by injecting small bubbles, in the case of elastic fluids this will leads to the formation of bubble clusters and therefore low values of the gas fraction and α. In that case, larger bubble sizes could be more convenient than small bubble sizes. In another paper we reported the formation of clusters in shear-thinning inelastic fluids having small bubbles [21]. However, the driving mechanism is different in both cases.

Acknowledgements

The authors thank Mariana Ramírez Gilly for her help with the rheological measurements. J.R. Vélez greatly acknowledges CONACyT-México for its financial support during his doctoral studies.

References

[1] O. Hassager, Negative wake behind bubbles in non-Newtonian liquids, Nature 279 (1979) 402.
[2] H.S. Dou, N. Phan-Thien, Negative wake in the uniform flow past a cylinder, Rheol. Acta 42 (2003) 383.
[3] J.R. Herrera-Velarde, R. Zenit, D. Chehata, B. Mena, The flow of non-Newtonian fluids around bubbles and its connection to the jump discontinuity, J. Non-Newtonian Fluid Mech. 111 (2003) 199.
[4] E. Soto, C. Goujon, R. Zenit, O. Manero, A study of velocity discontinuity for single air bubbles rising in an associative polymer, Phys. Fluids 18 (2006) 121510.
[5] D. Rodrigue, D. De Kee, Recent developments in the bubble velocity jump discontinuity, in: D. De Kee, R.P. Chhabra (Eds.), Transport Processes in Bubble, Drops, and Particles, second ed., Taylor & Francis, 2002.
[6] D.D. Joseph, Y.J. Liu, M. Poletto, J. Feng, Aggregation and dispersion of spheres falling in viscoelastic liquids, J. Non-Newtonian Fluid Mech. 54 (1994) 45.
[7] S. Mora, L. Talini, C. Allain, Structuring sedimentation in a shear-thinning fluid, Phys. Rev. Lett. 95 (2005) 088301.
[8] G. Astarita, G. Apuzzo, Motion of gas bubbles in non-Newtonian liquids, A.I.Ch.E. J. 11 (1965) 815.
[9] A. Acharya, R.A. Mashelkar, J. Ulbrecht, Mechanics of bubble motion and deformation in non-Newtonian media, Chem. Eng. Sci. 32 (1977) 863.
[10] Y.J. Liu, T.Y. Liao, D.D. Joseph, A two-dimensional cusp at the trailing edge of an air bubble rising in a viscoelastic liquid, J. Fluid Mech. 304 (1995) 321.
[11] M. Kemiha, X. Frank, S. Poncin, H.Z. Li, Origin of the negative wake behind a bubble rising in non-Newtonian fluids, Chem. Eng. Sci. 61 (2006) 4041.
[12] C. Pilz, G. Brenn, On the critical bubble volume at the rise velocity jump discontinuity in viscoelastic liquids, J. Non-Newtonian Fluid Mech. 145 (2007) 122.
[13] S.B. Pillapakkam, P. Singh, D. Blackmore, D. Aubry, Transient and steady state of rising bubble in a viscoelastic fluid, J. Fluid Mech. 589 (2007) 215.
[14] S.J. Lind, T.N. Phillips, The effect of viscoelasticity on a rising gas bubble, J. Non-Newtonian Fluid Mech. 165 (2010) 852.
[15] E. Zana, L.G. Leal, The dynamics and dissolution of gas bubbles in a viscoelastic fluid, Int. J. Multiph. Flow 4 (1978) 237.
[16] D. Rodrigue, D. De Kee, C.F. Chan Man Fong, An experimental study of the effect of surfactants on the free rise velocity of gas bubbles, J. Non-Newtonian Fluid Mech. 66 (1996) 213.
[17] D. Rodrigue, D. De Kee, C.F. Chan Man Fong, Bubble velocities: further developments on the jump discontinuity, J. Non-Newtonian Fluid Mech. 79 (1998) 45.
[18] K.J. Stebe, C. Maldarelli, Remobilizing surfactant retarded fluid particle interfaces II. Controling the surface mobility at interfaces of solutions containing surface active components, J. Colloid Int. Sci. 163 (1994) 177.
[19] L.G. Leal, Advanced Transport Phenomena, Fluid Mechanics and Convective Transport Processes, Cambridge University Press, Cambridge, 2010.
[20] M.T. Sullivan, K. Moore, H.A. Stone, Transverse instability of bubbles in viscoelastic channel flows, Phys. Rev. Lett. 101 (2008) 244503.
[21] J.R. Vélez-Cordero, R. Zenit, Bubble cluster formation in shear-thinning inelastic bubbly columns, J. Non-Newtonian Fluid Mech. 166 (2011) 32.
[22] J.R. Vélez-Cordero, D. Sámano, P. Yue, J.J. Feng, R. Zenit, Hydrodynamic interaction between a pair of bubbles ascending in shear-thinning inelastic fluids, J. Non-Newtonian Fluid Mech. 166 (2011) 118.
[23] D. Rodrigue, D. De Kee, Bubble velocity jump discontinuity in polyacrylamide solutions: a photographic study, Rheol. Acta 38 (1999) 177.
[24] R.B. Bird, R.C. Armstrong, O. Hassager, Dynamics of Polymeric Liquids, vol. 1, John Wiley & Sons, USA, 1987.
[25] D. Rodrigue, D. De Kee, C.F. Chan Man Fong, The slow motion of a single gas bubble in a non-Newtonian fluid containing surfactants, J. Non-Newtonian Fluid Mech. 86 (1999) 211.
[26] R.R. Lessard, S.A. Zieminski, Bubble coalescence and gas transfer in aqueous electrolytic solutions, Ind. Eng. Chem. Fundam. 10 (1971) 260.
[27] F. Calderas, A. Sanchez-Solis, A. Maciel, O. Manero, The transient flow of the PET–PEN–montmorillonite clay nanocomposite, Macromol. Symp. 283–284 (2009) 354.
[28] M. Stelter, G. Brenn, A.L. Yarin, R.P. Singh, F. Durst, Investigation of the elongational behavior of polymer solutions by means of an elongational rheometer, J. Rheol. 46 (2002) 507.

[29] M. Stelter, G. Brenn, A.L. Yarin, R.P. Singh, F. Durst, Validation and application of a novel elongational device for polymer solutions, J. Rheol. 44 (2000) 595.
[30] Y.J. Liu, D.D. Joseph, Sedimentation of particles in polymer solutions, J. Fluid Mech. 255 (1993) 565.
[31] D.D. Joseph, J. Feng, A note on the forces that move particles in a second-order fluid, J. Non-Newtonian Fluid Mech. 64 (1996) 299.
[32] M.C. Ruzicka, Vertical stability of bubble chain: multiscale approach, Int. J. Multiphase Flow 31 (2005) 1063.
[33] P. Vasseur, R.G. Cox, The lateral migration of spherical particles sedimenting in a stagnant bounded fluid, J. Fluid Mech. 80 (1977) 561.
[34] H.Z. Li, Y. Mouline, D. Funfschilling, P. Marchal, L. Choplin, N. Midoux, Evidence for in-line bubble interactions in non-Newtonian fluids, Chem. Eng. Sci. 53 (1998) 2219.
[35] G. Olivieri, M.E. Russo, M. Simeone, A. Marzocchella, P. Salatino, Effects of viscosity and relaxation time on the hydrodynamics of gas–liquid systems, Chem. Eng. Sci. 66 (2011) 3392.